

# Aerodynamic noise analysis of large horizontal axis wind turbines considering fluid–structure interaction

Hogeon Kim<sup>1</sup>, Seunghoon Lee<sup>1</sup>, Eunkuk Son<sup>1</sup>, Seungmin Lee<sup>1</sup>, Soogab Lee<sup>\*</sup>

Department of Mechanical and Aerospace Engineering, Institute of Advanced Aerospace Technology, Seoul National University, Rm. 318, Bldg. 313, Seoul National University, Seoul, 151-744, Republic of Korea

## ARTICLE INFO

### Article history:

Received 8 March 2011

Accepted 8 September 2011

Available online 7 October 2011

### Keywords:

Aerodynamic noise

Nonlinear composite beam theory

Nonlinear vortex correction method

Fluid–structure interaction

## ABSTRACT

Aerodynamic noise is one of the most serious barriers in wind energy development. To develop technologies for wind turbine noise reduction and assessment, noise needs to be predicted precisely with special consideration given to blade flexibility. The numerical tool, WINFAS, which can simulate fluid–structure interaction, consists of three parts: the first part, the Unsteady Vortex Lattice Method, analyzes aerodynamics; the second part, the Nonlinear Composite Beam Theory, analyzes structure; and the third part uses a semi-empirical formula to analyze airfoil self-noise and the Lawson's formula to analyze turbulence ingestion noise. In this study, using this numerical tool, the change in the noise strength due to blade flexibility was examined. This research showed that elastic blades decreased broadband noise because pitching motion reduced the angle of attack.

© 2011 Elsevier Ltd. All rights reserved.

## 1. Introduction

The wind energy industry is expanding rapidly around the world as a practical solution for Low-Carbon Green Growth. However, social and environmental problems such as landscape damage, shadow flicker, noise, electromagnetic interference and so on have remained as obstacles. Among them, noise has become the biggest problem [1].

Two kinds of approaches are mainly needed to resolve wind turbine noise. First, the generated noise needs to be reduced [2] and second, the extent of noise impact needs to be determined for post-compensation or pre-damage reduction during wind farm construction. To do this, we need a proper noise analysis and noise propagation method. The latest wind turbines are much larger than the previous ones. For example, in 1960s, the diameter of a wind turbine was only 40m; nowadays, it is over 120 m [3,4]. Since these large wind turbines are more flexible, aeroelastic deformation has to be considered in the wind turbine system analysis and design [5]. Moreover, in the past, aerodynamic noise analysis has always assumed a rigid blade but now, they need to consider a flexible blade. The purpose of this study is to investigate the effects of the deformation of a large wind turbine blade on aerodynamic noise.

To assess the effects of blade flexibility on aerodynamic noise, three kinds of methods are used. The Nonlinear Vortex Correction Method [6], based on the Unsteady Vortex Lattice Method, is used for the aerodynamic analysis of the wind turbine beyond the stall region, and the Nonlinear Composite Beam Theory developed by Hodges [7,8] is used for the structure analysis. Finally, Turbulent Ingestion (TI) noise [9] and Turbulent Boundary Layer Trailing Edge [10] noise are analyzed with information on the blade deformation and flow field.

## 2. Numerical method

Fig. 1 shows the schematic diagram of wind turbine blade aerodynamic noise analysis considering fluid–structure Interaction (FSI). The analysis method consists of three parts: aerodynamic part, structural part, and aeroacoustic part. The Nonlinear Vortex Correction Method (NVCM), which is based on the Unsteady Vortex Lattice Method (UVLM), is used for the aerodynamic analysis in the stall region. The Nonlinear Composite Beam Theory (NCBT) that D.H. Hodges derived is used for the structural analysis. In order to improve the convergence of the aerodynamic and structural solutions, the structural code is converged first for the condition of vacuum state, and a loosely coupled analysis is carried out with increase from zero to full load for 1 revolution. After the pre-convergence procedure, the full load condition is applied to calculate the FSI. In this research, a total of 10 revolutions are performed with full load.

<sup>\*</sup> Corresponding author. Tel.: +82 2 880 7384; fax: +82 2 875 4360.

E-mail address: [solee@snu.ac.kr](mailto:solee@snu.ac.kr) (S. Lee).

<sup>1</sup> Tel.: +82 2 880 7545.

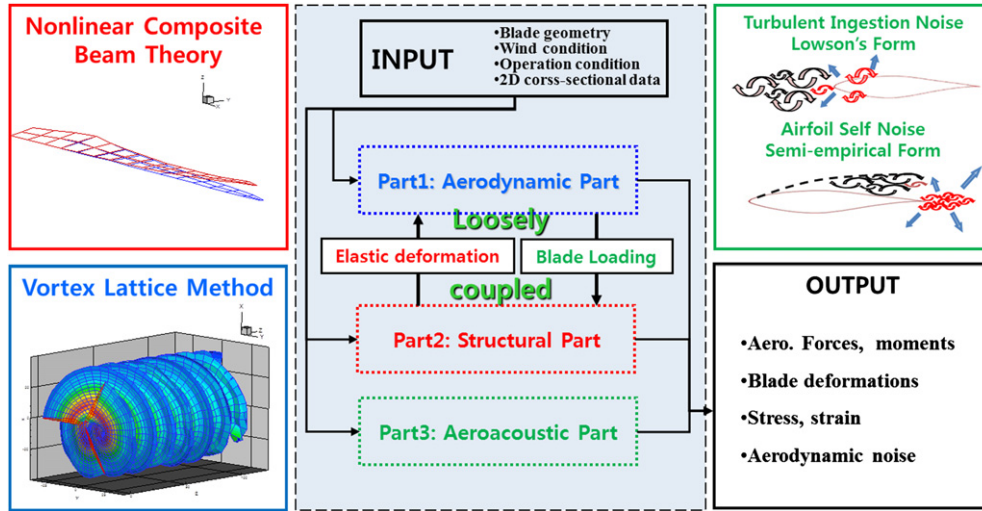


Fig. 1. Schematic procedure of wind turbine aerodynamic noise analysis considering FSI.

After the FSI calculation, aerodynamic noise analysis is performed using blade deformation, effective angle of attack, and onset velocity on each blade section. Because the main sources of wind turbine aerodynamic noise are Turbulent Ingestion (TI) noise and Turbulent Boundary Layer Trailing Edge (TBL-TE) noise, we analyzed two noise sources in this study.

### 2.1. Nonlinear vortex correction method

The UVLM based on potential flow cannot calculate thickness and viscous effects. Therefore, a two-dimensional table should be used [11,12] to consider these effects inherently. However, a two-dimensional table yields an incorrect angle of attack and aerodynamic coefficients because the UVLM evaluates the bound circulations on the lifting surface without regard to thickness and viscous effects of airfoil. That error is corrected by matching up the sectional lift from the UVLM with that from the two-dimensional table look-up [6].

The NVCM is summarized as follows:

Initial Stage: If  $F = dL_{UVLM} - dL_{table\ look-up} \neq 0$

then:  $\Gamma_{initial} \pm \Delta\Gamma \rightarrow \Gamma_{modified}$

Final Stage: If  $F \rightarrow 0$ , then use  $\Gamma_{modified}$

where  $dL_{UVLM}$  and  $dL_{table\ look-up}$  indicate sectional lift from the UVLM and the table look-up procedure, respectively;  $F$  is the difference between these two values; and  $\Gamma$  indicates the bound vortex strength of the blade span wise section. Using the unsteady Bernoulli equation and the pressure difference,  $dL_{UVLM}$  is computed from the UVLM. In this research, to consider a three-dimensional stall delay, AirfoilPrep [13] was used. The local effective angle of attack and the Reynolds number were calculated using the UVLM. Then,  $dL_{table\ look-up}$ , sectional drag and sectional pitching moment were obtained by interpolation from the airfoil data table according to the calculated effective angle of attack and the Reynolds number.

If  $F$  is not zero,  $F$  is modified by the matching process between  $dL_{UVLM}$  and  $dL_{table\ look-up}$  using addition or subtraction of  $\Delta\Gamma$ , which is equal value in one span wise section. However, in this matching process, the bound vortex strength cannot be determined by matching because of the nonlinearity between the bound vortex strength and the angle of attack for not only independent strips but

also neighboring blade strips. For this reason, this process has to be represented by a nonlinear system of equations:

$$\begin{aligned} F_1(x) &= (dL_{UVLM})_1 - (dL_{table\ look-up})_1 \\ F_2(x) &= (dL_{UVLM})_2 - (dL_{table\ look-up})_2 \\ &\vdots \\ F_n(x) &= (dL_{UVLM})_n - (dL_{table\ look-up})_n \end{aligned} \quad (1)$$

where  $x_1 = \Delta\Gamma_1$ ,  $x_n = \Delta\Gamma_n$  and  $x = (x_1, x_2, \dots, x_n)$ . Subscript  $n$  is the total number of blade span wise sections. The vector form of Eq. (1) is given by

$$F(x) = 0 \quad (2)$$

Eq. (2) can be solved by applying by a sophisticated Newton–Raphson iterative method having a rapid local convergence algorithm and a global convergent strategy [14]. The wake shed from the trailing edge is described using a vortex ring to predict wake convection. At each time step, the free wake moves at the total velocity.

### 2.2. Nonlinear composite beam theory

Rotating beam coordinate systems are shown in Fig. 2. Coordinate ‘a’ is the global frame, with its axes labeled  $a_1$ ,  $a_2$ , and  $a_3$  are rotating with the rotor. The undeformed blade coordinate is the ‘b’ frame. Blade’s deformed frame is named ‘B’ with its axes  $B_1$ ,  $B_2$ , and  $B_3$ .

An arbitrary vector  $U$  that is in the ‘a’ frame can be expressed by its components in the ‘B’ or ‘b’ frame using the transformation matrices below

$$U_B = C^{Ba}U_a, \quad U_b = C^{ba}U_a \quad (3)$$

where  $C^{Ba}$  is the transformation matrix from ‘a’ to ‘B’, and  $C^{ba}$  is that from ‘a’ to ‘b’.

A mixed form of the variational equation is used for the modeling of the blade structure. Hamilton’s principle is used to derive the mixed form of the variational equation,

$$\int_{t_1}^{t_2} \int_0^l [\delta(K - U) + \delta W] dx_1 dt = \delta A \quad (4)$$

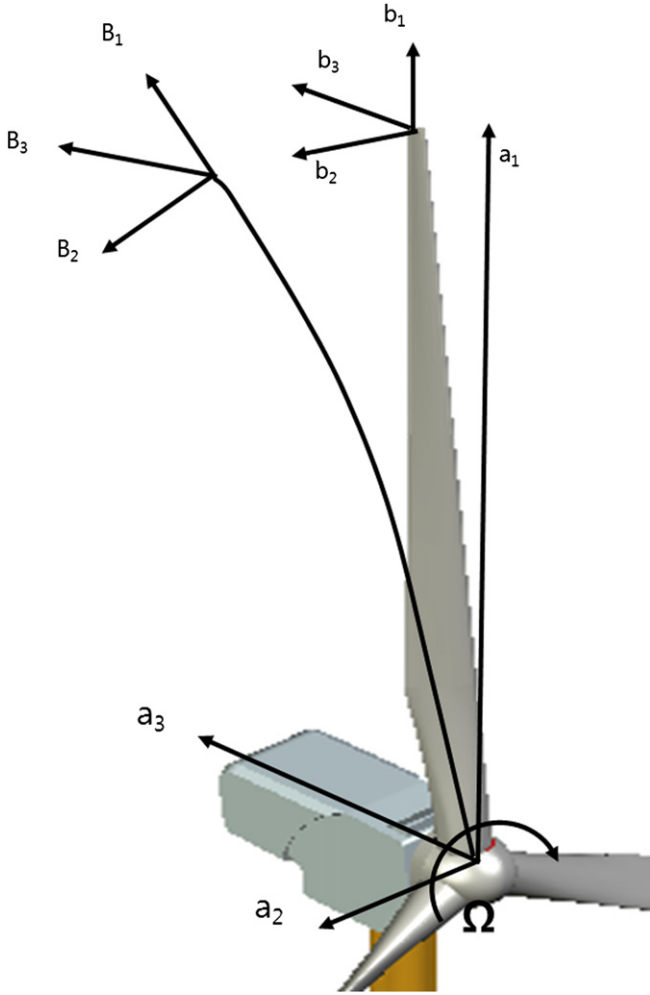


Fig. 2. Coordinates system for moving beam dynamics. 'a' frame is global coordinate rotating with rotor. 'b' frame is undeformed blade coordinate. 'B' is blade's deformed frame.

where  $t_1$  and  $t_2$  are arbitrary fixed times, and  $l$  means the length of the beam.  $K$  and  $U$  are the kinetic energy and potential energy per unit length.  $\delta A$  is the virtual action at the ends of the beam during a time interval.  $\delta W$  is the virtual work of applied loads per unit length. Partial derivatives of  $U$  and  $K$  with respect to  $\gamma$ ,  $\kappa$ ,  $V_B$  and  $\Omega_B$  are the internal force and moment vectors  $F_B$  and  $M_B$ , and the linear and angular momentum vectors  $P_B$  and  $H_B$  are defined as

$$F_B = \left( \frac{\partial U}{\partial \gamma} \right)^T, \quad M_B = \left( \frac{\partial U}{\partial \kappa} \right)^T, \quad P_B = \left( \frac{\partial K}{\partial V_B} \right)^T, \quad H_B = \left( \frac{\partial K}{\partial \Omega_B} \right)^T \quad (5)$$

where  $\gamma$  and  $\kappa$  are the force and momentum strain and  $V_B$  and  $\Omega_B$  are the linear and angular velocities, respectively. The first term of  $F_B$  is the axial force ( $B_1$  axis, outward direction from the root to tip) and the second and third terms are the shear force. By same convention of  $F_B$ , the first term of  $M_B$  is the torsional moment, and the second and third terms of  $M_B$  are the bending moment (more details in Ref. [8]).

For mixed variational form, Lagrange's multipliers are used and the complete variational formulation can be derived in the 'a' frame based on the geometrically exact equation.

$$\int_{t_1}^{t_2} \delta \Pi_a dt = 0$$

$$\delta \Pi_a = \int_{t_1}^{t_2} \left\{ \delta u_a^T C^T C^{ab} F_B + \delta u_a^T \left[ \left( C^T C^{ab} P_B \right)' + \tilde{\omega}_a C^T C^{ab} P_B \right] \right. \\ + \delta \bar{\psi}' C^T C^{ab} M_B - \delta \bar{\psi} C^T C^{ab} (\tilde{e}_1 + \tilde{\gamma}) F_B \\ + \delta \bar{\psi}_a^T \left[ \left( C^T X C^{ab} H_B \right) + \tilde{\omega}_a C^T C^{ab} H_B + C^T C^{ab} \tilde{V}_B P_B \right] \\ - \delta \bar{F}_a^T \left[ C^T C^{ab} (e_1 + \gamma) - C^{ab} e_1 \right] - \delta \bar{F}_a^T u_a \\ - \delta \bar{M}_a^T \left( \Delta + \frac{\tilde{\theta}}{2} + \frac{\theta \theta^T}{4} \right) C^{ab} k - \delta \bar{M}_a^T u_a \\ + \delta \bar{P}_a^T \left( C^T C^{ab} V_B - V_a - \tilde{\omega}_a u_a - \delta \bar{P}_a^T \dot{u}_a \right) \\ + \delta \bar{H}_a^T \left( \Delta - \frac{\tilde{\theta}}{2} + \frac{\theta \theta^T}{4} \right) \left( C^T C^{ab} + \Omega_B - \omega_a \right) \\ \left. - \delta \bar{H}_a^T \dot{\theta} - \delta u_a^T f_a - \delta \bar{\psi}_a^T m_a \right\} dx_1 \\ - \left( \delta u_a^T \hat{F}_a + \delta \bar{\psi}_a^T \hat{M}_a - \delta \bar{F}_a^T \hat{u}_a - \delta \bar{M}_a^T \hat{\theta}_a \right) \Big|_0^l \quad (6)$$

where  $f_a$  and  $m_a$  are the aerodynamic force and moment vector.  $\delta u_a^T f_a - \delta \bar{\psi}_a^T m_a$  is the virtual work of the aerodynamic load per unit length.  $\hat{F}_a$ ,  $\hat{M}_a$ ,  $\hat{u}_a$  and  $\hat{\theta}_a$  are the boundary conditions. For the wind turbine case,  $\hat{F}_a$  and  $\hat{M}_a$  of the blade tip are zero and  $\hat{u}_a$  and  $\hat{\theta}_a$  of the blade root are zero (see more details in Ref. [8]).

For finite element discretization, the blade is divided into  $N$  elements, and Eq. (6) can be rewritten as

$$\int_{t_1}^{t_2} \sum_{i=1}^N \delta \Pi_i dt = 0 \quad (7)$$

where  $i$  is an  $i$ th element of length  $dl$  and  $\delta \Pi_i$  is the corresponding spatial integration over the  $i$ th element of Eq. (6). Because Eq. (7) was derived by the mixed variational formulation, simple shape functions can be used. Substitutions and interpolations such as Eq. (8) are carried out on each element.

$$x = x_i + \xi \Delta l_i, \quad dx = \Delta l_i d\xi, \quad (') = \frac{1}{\Delta l_i} \frac{d}{d\xi} ( )$$

$$\delta u_a = \delta \hat{u}_i (1 - \xi) + \delta \hat{u}_{i+1} \xi, \quad u_a = \hat{u}_i$$

$$\delta \bar{\psi}_a = \delta \bar{\hat{\psi}}_i (1 - \xi) + \delta \bar{\hat{\psi}}_{i+1} \xi, \quad \theta = \hat{\theta}_i$$

$$\delta \bar{F}_a = \delta \bar{\hat{F}}_i (1 - \xi) + \delta \bar{\hat{F}}_{i+1} \xi, \quad F_B = \hat{F}_i$$

$$\delta \bar{M}_a = \delta \bar{\hat{M}}_i (1 - \xi) + \delta \bar{\hat{M}}_{i+1} \xi, \quad m_B = \hat{M}_i$$

$$\delta \bar{P}_a = \delta \hat{P}_i, \quad P_B = \hat{P}_i$$

$$\delta \bar{H}_a = \delta \hat{H}_i, \quad H_B = \hat{H}_i \quad (8)$$

where  $\xi$  is a value from 0 to 1.

Using Eqs. (6)–(8), the structural and aerodynamic parts can be discretized to simplify the resulting equations as follows

$$F_S(X, \dot{X}) - F_L = 0 \quad (9)$$

where  $F_S$  is the structural operator,  $F_L$  is the aerodynamic operator, and  $X$  is the unknown vector. A second-order backward Euler method is applied for time integration, and a nonlinear algebraic equation at  $n$ th time step can be obtained.

$$F_s(X^n) - F_L = 0 \quad (10)$$

Eq. (10) can be solved using Newton's method. The solutions of Eq. (10) are displacement, stress and strain at each time step.

### 2.3. Aerodynamic noise model

Effective angles of attack, onset velocities and deformations, which are calculated by using FSI, are used to analyze wind turbine aerodynamic noise. In this study, the Turbulent Ingestion noise (TI) [9] is predicted using Lowson's model and the Turbulent Boundary Layer Trailing Edge noise (TBL-TE) is predicted by using the Semi-Empirical formula [10] because TI and TBL-TE noises are the main sources of wind turbine aerodynamic noise. Boundary layer displacement thickness data needed to calculate the TBL-TE noise are tabulated and categorized according to Reynold's number, angle of attack, onset velocity and  $r/R$  using Xfoil [15].

The TI noise is generated by the interaction of atmospheric turbulence with the rotor blade because of pressure fluctuations. High and low frequency TI noises can be analyzed by Eq. (11), in which Lowson [9] adopted the model of Amiet [16]

$$\begin{aligned} \text{SPL}_{\text{TIN}}^{\text{H}} &= 10 \log_{10} \left[ \rho^2 c_0^2 L \frac{\Delta l}{r^2} M^3 I^3 k^3 (1 + k^2)^{7/3} \right] + 58.4 \\ \text{SPL}_{\text{TIN}}^{\text{L}} &= \text{SPL}_{\text{TIN}}^{\text{H}} + 10 \log_{10} \left( \frac{k_{\text{lf}}}{1 + k_{\text{lf}}} \right) \\ k &= \pi f c / V, \quad \beta^2 = 1 - M^2, \quad K_{\text{lf}} = 10 S^2 M K^2 / \beta^2, \\ S^2 &= \left( \frac{2\pi k}{\beta^2} + \frac{1}{1 + 2.4k/\beta^2} \right) \end{aligned} \quad (11)$$

where  $k_{\text{lf}}$  is the low frequency correction factor,  $\rho$  is the density of air,  $M$  is the Mach number,  $V$  is the onset velocity,  $c_0$  is the speed of sound,  $I$  indicates the turbulence intensity and  $L$  indicates the length scale of turbulence.

A boundary layer develops on the blade surface. Laminar flow transitions to turbulent flow and the turbulence of the boundary layer induces a fluctuating pressure field in time and space. When turbulent eddies meet a sharp edge like a trailing edge, they become more efficient as sound sources. The TBL-TE noise can be predicted by Eq. (12)

$$\text{SPL}_{\text{TEL-TE}} = 10 \log_{10} \left[ 10^{\text{SPL}_s/10} + 10^{\text{SPL}_p/10} + 10^{\text{SPL}_\alpha/10} \right] \quad (12)$$

where  $\text{SPL}_s$  is the TBL-TE noise induced by the suction side, and  $\text{SPL}_p$  is the TBL-TE noise contributed by the pressure side [10]. The last term of Eq. (12),  $\text{SPL}_\alpha$ , is the TBL-TE noise due to the shed turbulent vorticity that occurs when the flow separates near the trailing edge for nonzero angles of attack. The three terms of Eq. (12) are

$$\begin{aligned} \text{SPL}_s &= 10 \log_{10} \left( \frac{\delta_s^* M^5 D_h \Delta l}{r^2} \right) + G_A \left( \frac{St_s}{St_1} \right) + W_1 - 3 \\ \text{SPL}_p &= 10 \log_{10} \left( \frac{\delta_p^* M^5 D_h \Delta l}{r^2} \right) + G_A \left( \frac{St_p}{St_1} \right) + W_1 - 3 + \Delta W \\ \text{SPL}_\alpha &= 10 \log_{10} \left( \frac{\delta_s^* M^5 D_h \Delta l}{r^2} \right) + G_B \left( \frac{St_s}{St_2} \right) + W_2 \end{aligned} \quad (13)$$

where  $\delta_s^*$  and  $\delta_p^*$  are the suction and pressure side boundary layer displacement thickness,  $D_h$  is the directivity function,  $M$  is the Mach number,  $G_A$  and  $G_B$  are the spectral shape functions,  $W_1$  and  $W_2$  are the amplitude functions and  $\Delta W$  is the level adjustment amplitude

function for nonzero angles of attack (more explanations about other parameters are in Ref. [10]).

## 3. Results and discussion

### 3.1. Validation

Unfortunately, there are no data to validate the aerodynamic, structural and aeroacoustic results of this study at once. Therefore, the results of three parts of WINFAS were validated separately.

The comparison of low speed shaft torques of the NREL Phase VI experiments [17–19] is shown in Fig. 3. The results calculated by the NVCM of WINFAS are in good agreement with the experiments.

In order to validate the structural analysis part of WINFAS, flapwise tip displacement of WINFAS was compared with that of other numerical tools. RB 70 rotor blade [22] of radius 35.2 m and rated power 1.5 MW was used for the validation of the structural part of WINFAS. As seen Fig. 4, WINFAS' results are good consistent with the results of other numerical tools.

The noise prediction part of WINFAS was validated by comparison with noise measurements [23], as seen in Figs. 5 and 6. Fig. 5 indicates good agreement between the sound power level (LWA) of the experiments and that of the simulation. Though by spectrum comparison in Fig. 6, differences are observed in some frequency regions, it can be seen good agreement generally. Note that NM-72 is the active stall control type and several peaks in the measurement spectrum can come from the mechanical part of the wind turbine such as the gearbox.

### 3.2. Noise calculation

The rotor of the 3 MW wind turbine system, which has three blades of radius 45.8 m and rated wind speed 12.5 m/s at 15.7 rated rpm, was used for the aerodynamic noise calculation. Airfoils of the blade consist of DU series, whose thickness ratio is from 40% to 20% and NACA64-618 in the tip region. The blade was divided up into

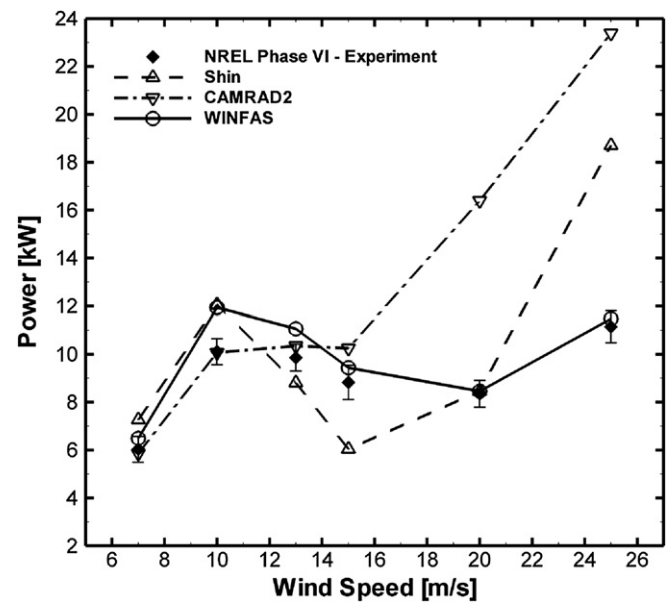


Fig. 3. Low speed shaft torque comparison with NREL Phase VI experiment [17–19]. Shin used the vortex lattice method based on free wake without post stall consideration [20]. CAMRAD2 is based on Lifting Line Method [21].

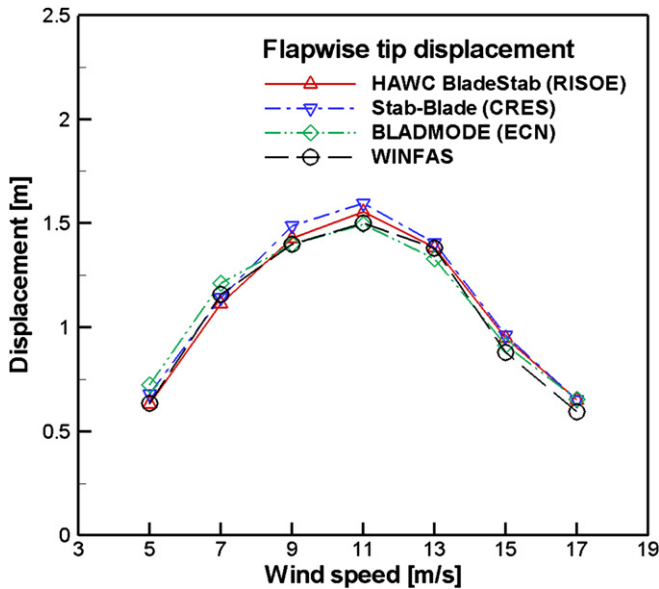


Fig. 4. Comparison of flapwise blade tip deformation of RB 70 [22]. HAWCBladeStab is program of Risø used for the aeroelastic stability analysis of blade vibrations; Stab-Blade is program of CRES for the aeroelastic stability analysis of blade vibrations; and BLADMODE is program of ECN for the rotor blade eigenmode analysis.

15 vortex lattices along the radial directions and 2 vortex lattices along the chordwise directions for simulation. An azimuthal step size is 6°.

The aerodynamic power difference, which is normalized by the power with consideration of the FSI, is about 5% over 10.5 m/s. Blade deformation changes the effective angle of attack and onset velocity. Especially, blade pitching down due to blade flexibility would have the biggest effect on the decrease of the angle of attack. Its decrease would reduce the aerodynamic load as shown in Fig. 7.

Fig. 8 describes the difference between the SPL of a flexible blade and that of a rigid blade. In contrast to the tendency of aerodynamic power due to blade flexibility, the tendency of noise level shows no

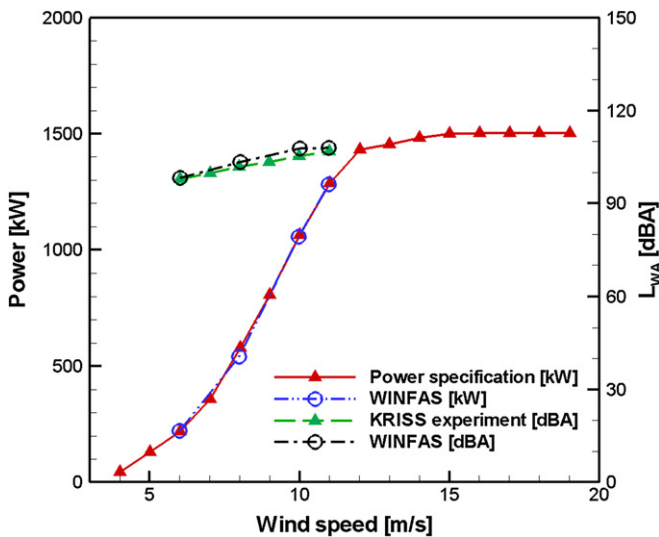


Fig. 5. Power and sound power level of NM-72 per wind speed. Specification means the power curve provided by NEG-Micon. Noise measurement was performed by KRISS detailed in Ref. [23].

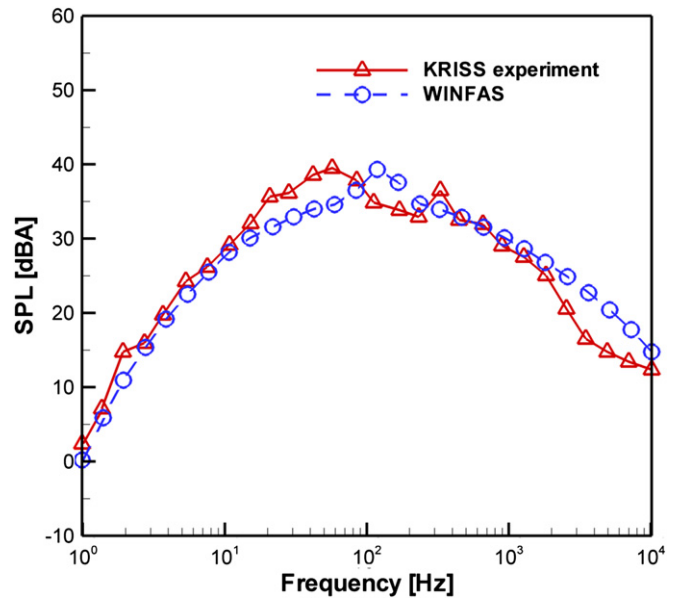


Fig. 6. One-third octave band spectrum in 6 m/s. Noise measurement was performed by KRISS detailed in Ref. [23].

significant difference by blade deformation for wind speeds over 14.5 m/s. The rotor rotational speed of most modern large wind turbines reaches the rated RPM when the wind speed is just below 1–2 m/s of the rated speed. Moreover, pitch control maintains the electric power at a constant level when the wind speed is over the rated wind speed.

Therefore, because the wind turbine blade operates in the condition of low angle of attack at wind speeds over 12.5 m/s, the difference in the angle of attack by pitching down does not have significant effect on the aerodynamic noise. Moreover, because the velocity due to rotation, which is a component of the total onset

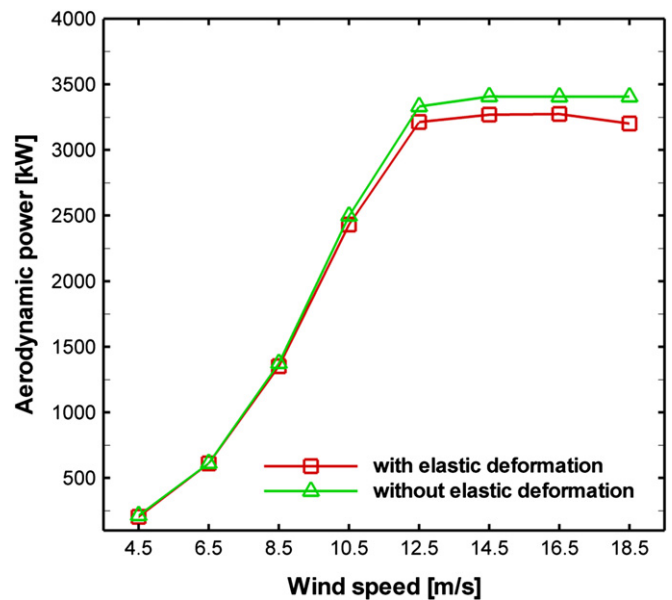


Fig. 7. Aerodynamic power considering elastic deformation. Normalized differences between power of case without deformation and that of case with deformation are about 5% over wind speed of 10.5 m/s.

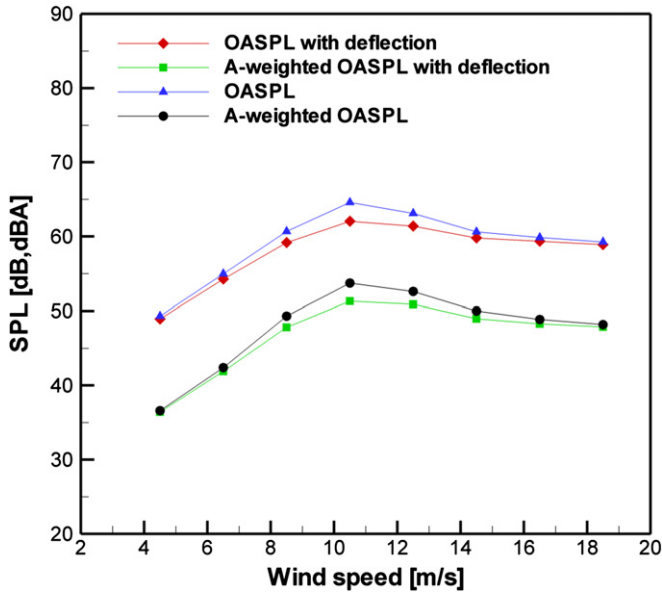


Fig. 8. Sound pressure level of various wind speed cases in uniform flow. At the rated wind speeds, 11.5 m/s and 10.5 m/s, the SPL difference between the case considering deflection and that not considering deflection is about 2–1.5 dB.

velocity on each section, is constant over the rated wind speed, the TBL-TE noise does not change significantly.

Important parameters describing the TI noise are the turbulence intensity, the length scale of turbulence and onset velocity. However, the fluid–structure interaction of the wind turbine blades does not change the values of these parameters. Therefore, the differences in the TI noise, which contribute to the total noise (overall SPL) between the elastic and rigid rotor cases, are not significant (Fig. 9a, b). Though the overall SPL changes slightly due to the blade elasticity in the low frequency region (<200 Hz), this amount of change is meaningless for A-weighted noise level.

Fig. 10(a) and (b) show the frequency spectrum of the TBL-TE noise considering the FSI at 10.5 m/s and 18.5 m/s. As seen in Fig. 10(b), the TBL-TE<sub>z</sub> and TBL-TE<sub>s</sub> noise increase because of blade deflection at wind speed of 10.5 m/s. When the wind speed is 18.5 m/s, the angle of attack reduced by tensorial deflection does not change the TBL-TE noise significantly as mentioned above, because the tip and mid regions of the blade have a low angle of attack. SPL footprint is shown in Figs. 11 and 12 on the flat terrain. The sound power level predicted in rigid blade condition is higher than that calculated in the flexible blade condition near wind turbine position, (x, y) = (0, 0).

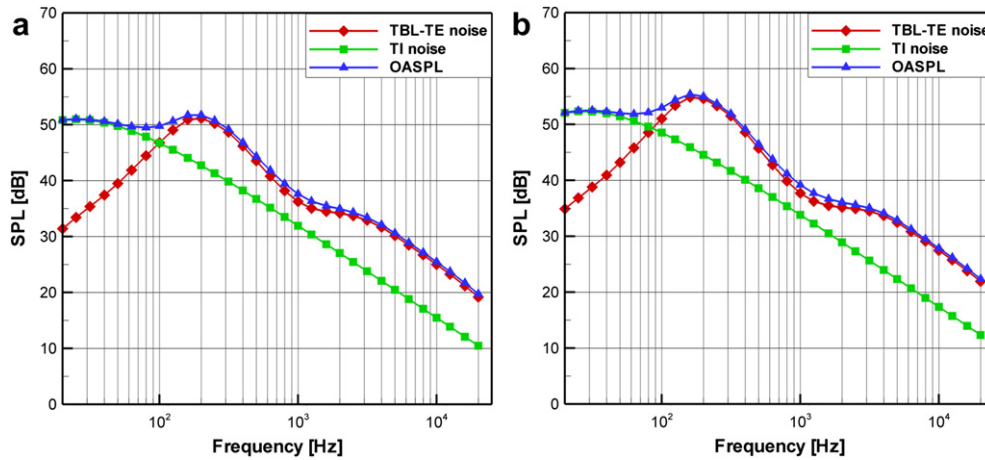


Fig. 9. Frequency spectrum of TI noise at wind speed of 10.5 m/s with deflection (a) and without deflection (b).

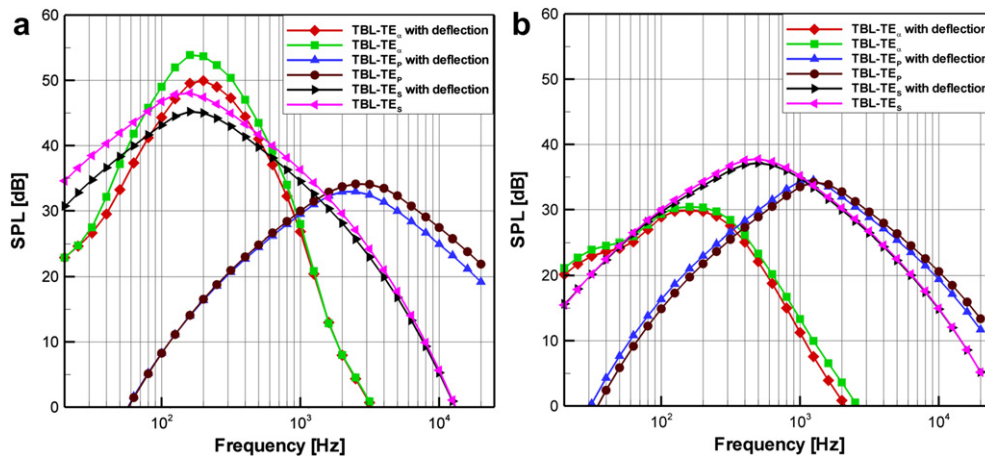


Fig. 10. Frequency spectrum of TBL-TE noise at wind speed of 10.5 m/s (a) and at wind speed of 18.5 m/s (b). TBL-TE<sub>p</sub> is turbulent boundary layer pressure side noise. TBL-TE<sub>s</sub> indicates turbulent boundary layer suction side noise. TBL-TE<sub>z</sub> is separated flow noise.

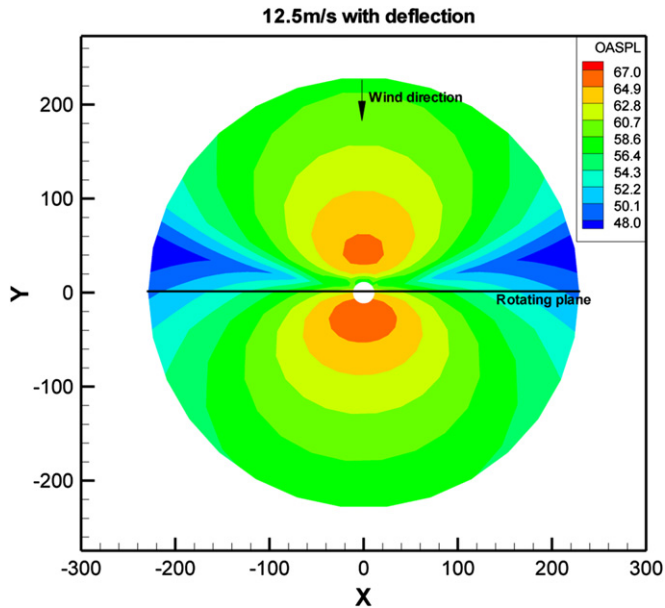


Fig. 11. Footprint of overall sound pressure level with deflection in wind speed of 12.5 m/s.

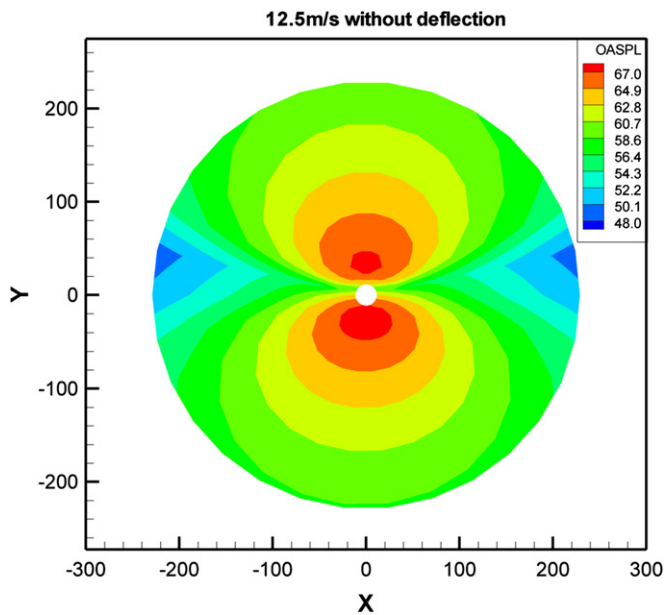


Fig. 12. Footprint of overall sound pressure level without deflection in wind speed of 12.5 m/s.

#### 4. Conclusions

This paper described the effects of blade flexibility on aerodynamic noise. For considering fluid–structure interaction, the NVCN was used for aerodynamic analysis and the Nonlinear Composite Beam Theory was applied for structural dynamics modeling. Finally, the flow parameters such as effective angle of attack, blade deformed geometry and onset velocity, calculated by the numerical method with or without FSI, were used for the prediction of aerodynamic noise, namely, TI noise and TBL-TE noise. At 8–12 m/s of uniform flow, the sound pressure level with consideration of blade deflection was about 1.5–2.5 dB, which was

low compared to that of a rigid blade. When wind speed was over 12 m/s, the rated wind speed, noise was not changed significantly by blade flexibility because the wind turbine blade operated in the low angles of attack range in the mid and tip regions of the blade due to pitch control that modern large wind turbines have. In other words, the angle of attack changes in the condition of low angle of attack, around  $0^\circ$ , produces smaller variations of noise level than that in the condition of high angle of attack, around  $5^\circ$ . With respect to noise assessment, this method takes too long to predict the noise produced by a modern large wind turbine considering FSI. Therefore, at wind speeds in which blade flexibility affects the aerodynamic noise, overpredicted sound pressure levels that a rigid blade generates should be corrected.

This research was limited to the pitch-controlled variable speed wind turbine under the steady uniform flow condition. Future research will study the blade flexibility effect on noise generated by different types of wind turbine systems under individual pitch control, stall control, unsteady wind condition, and time-dependent wind velocity.

#### Acknowledgements

This work was supported by the Human Resources Development and the New and Renewable Energy of the Korea Institute of Energy Technology Evaluation and Planning (KETEP) grant funded by the Korea Ministry of Knowledge and Economy (nos. 20094020100060 & 20104010100490).

#### References

- [1] Johansson L. Summary of IEA topical expert meeting on noise immission; 2000.
- [2] Kim T, Lee S, Kim H, Lee S. Design of low noise airfoil with high aerodynamic performance for use on small wind turbines. *Sci China Tech Sci* 2010;53:75–9.
- [3] Harrison R, Hau E, Snel H. Large wind turbine: design and economics. West Sussex, England: John Wiley & Sons Ltd; 2000. pp.1–26.
- [4] EWEA. Wind energy – the facts. Part I: technology. European Wind Energy Association; 2009. 72–79.
- [5] Hansen MOL, Sørensen JN, Voutsinas S, Sørensen N, Madsen HA. State of the art in wind turbine aerodynamics and aeroelasticity. *Prog Aerospace Sci* 2006; 42:285–330.
- [6] Kim H, Lee S, Lee S. Numerical analysis on the aerodynamics of HAWTs using nonlinear vortex strength correction. *Curr Appl Phys* 2010;10:s311–5.
- [7] Hodges DH, Yu W, Rigorous A. Engineer-friendly approach for modelling realistic, composite rotor blades. *Wind Energy* 2007;10:179–93.
- [8] Shang X, Hodges DH, Peters DA. Aeroelastic stability of composite hingless rotors in hover with finite-state unsteady aerodynamics. *J Am Helicopter Soc* 1999;44:206–21.
- [9] Lowson MV. Assessment and prediction model for wind turbine noise: basic aerodynamic and acoustic models, flow solution report; 1993.
- [10] Brooks FT, Pope DS, Marcolini MA. Airfoil self-noise and prediction. NASA Reference Publication; 1989.
- [11] Prandtl L, Tietjens OG. Applied hydro-and aeromechanics. New York, USA: DOVER; 1934.
- [12] van Garrel A. Development of wind turbine aerodynamics simulation module. ECN-C-03-079; 2003.
- [13] NWTC design codes (AirfoilPrep by Dr. Craig Hansen). Available from: <http://wind.nrel.gov/designcodes/preprocessors/airfoilprep/>. Last [modified/accessed 16 January 2007].
- [14] Press WH, Teukolsky SA, Vetterling WT, Flannery BP. In: Numerical recipes in Fortran: the art of scientific computing. 2nd ed. Cambridge, England: Cambridge University Press; 1992. p. 372–86.
- [15] Drela M. An analysis and design system for low reynolds number airfoils. Conference on low Reynolds number aerodynamics; 1989.
- [16] Amiet RK. Acoustic radiation from an airfoil in a turbulent stream. *J Sound Vibration* 1975;41:407–20.
- [17] Hand MM, Simms DA, Fingersh LJ, Jager DW, Cotrell JR, Schreck S, Larwood SM. Unsteady aerodynamics experiment phase VI: wind tunnel test configurations and available data campaigns. NREL/TP-500-29955; 2001.
- [18] Simms DA, Schreck S, Hand MM, Fingersh LJ, Cotrell JR, Pierce K, Robinson M. Plans for testing the NREL unsteady aerodynamics experiment 10-m diameter HAWT in the NASA Ames wind tunnel. NREL/TP-500-27599; 1999.
- [19] Simms DA, Schreck S, Hand MM, Fingersh LJ. Unsteady aerodynamics experiment in the NASA-Ames wind tunnel: comparison of predictions to measurements. NREL/TP-500-29494; 2001.

- [20] Shin H. Numerical and experimental analysis of performance, aerodynamic load and noise on HAWT blade. Ph.D. dissertation, Department of Aerospace Engineering, Seoul National University; 2005.
- [21] Duque EPN, Burklund MD, Johnson W, Navier–Stokes and comprehensive analysis performance predictions of the NREL phase VI experiment. AIAA paper no. 2003-0355, ASME wind energy symposium; 2003. p. 1–19.
- [22] Lindenburg C. Structural pitch for a pitch-to-vane controlled wind turbine rotor. ECN-C-03-087; 2004.
- [23] Lee S, Cheong C. Experimental investigation into infrasound and low-frequency noise radiation characteristics from large wind turbines. The Korean Society for Noise and Vibration Engineering; 2007. 07A-53-03.